The Astrophysical Journal Letters, 998:L8 (7pp), 2026 February 10 https://doi.org/10.3847/2041-8213/ae3b3e

Ancient Relic Moderately Metal-rich Bulge Cluster Tonantzintla 2

Sergio Ortolani[1,2,3], Stefano O. Souza[4], Domenico Nardiello[1,3], Beatriz Barbuy[5], Eduardo Bica[6], Bernardo P.L. Ferreira[5], Cristina Chiappini[7], José G. Fernández-Trincado[8], and Heitor Ernandes[9]
[1] Dipartimento di Fisica e Astronomia, Università di Padova, Vicolo dell'Osservatorio 2, Padova, 35122, Italy
[2] Centro di Ateneo di Studi e Attività Spaziali "Giuseppe Colombo," Via Venezia 15, Padova, 35131, Italy
[3] INAF—Osservatorio di Padova, Vicolo dell'Osservatorio 5, Padova, 35122, Italy
[4] Max Planck Institute for Astronomy, Königstuhl 17, D-69117 Heidelberg, Germany
[5] Universidade de São Paulo, IAG, Rua do Matão 1226, Cidade Universitária, São Paulo 05508-900, Brazil; b.barbuy@iag.usp.br
[6] Universidade Federal do Rio Grande do Sul, CP 15051, Porto Alegre, 91501-970, Brazil
[7] Leibniz Institute for Astrophysics, An der Sternwarte 16, Potsdam, 14482, Germany
[8] Universidad Católica del Norte, Núcleo UCN en Arqueología Galáctica—Inst. de Astronomía, Av. Angamos 0610, Antofagasta, Chile
[9] Lund Observatory, Department of Geology, Lund University, Sölvegatan 12, Lund, Sweden
Received 2025 December 23; revised 2026 January 19; accepted 2026 January 19; published 2026 February 4

Abstract

The assembly history of the Galactic bulge is intimately tied to the formation of the proto–Milky Way, yet reconstructing this early phase is difficult because mergers and secular evolution have erased most of its original structure. Among present-day stellar systems, only globular clusters retain the ancient signatures needed to trace these primordial building blocks. Here we present the most detailed characterization to date of Tonantzintla 2, a prime candidate for a relic of the Milky Way's primordial bulge. It is a moderately metal-rich globular cluster projected onto the bulge that has remained largely unexplored despite its potential to constrain the early formation of the inner Milky Way. We derive its fundamental parameters using proper-motion-corrected Hubble Space Telescope WFC3 and Advanced Camera for Surveys photometry. By applying an isochrone fitting to very clean data, we obtain an age of $13.58^{+0.72}_{-1.0}$ Gyr, a reddening $E(B-V) = 1.44 \pm 0.02$, a metallicity $[M/H] = -0.68^{+0.04}_{-0.05}$, and a heliocentric distance of $d_{\odot} = 7.38^{0.13}_{0.08}$ kpc. A complementary chemical-abundance analysis of seven member stars from APOGEE high-resolution spectroscopy reveals an enrichment pattern consistent with an in situ origin. Tonantzintla 2 is among the oldest globular clusters studied in the literature, and the oldest so far analyzed in the Galactic bulge. Its age places a stringent constraint on the onset of the bulge formation, implying that star formation in the inner Galaxy began within ∼0.2 Gyr of the Big Bang and that Tonantzintla 2 represents an exceptional relic of the Milky Way's earliest chemical enrichment.

Unified Astronomy Thesaurus concepts: Globular star clusters (656); Galaxy ages (576)

1. Introduction

The moderate-metallicity globular clusters ($-1.4 < [Fe/H] < -0.2$) projected in the direction of the Galactic bulge are ancient systems that should trace the earliest phases of the Milky Way's formation. E. Bica et al. (2024) reported an updated census of bulge globular clusters, together with their metallicities and ages. Yet for a significant fraction of the moderately metal-rich ($-0.8 < [Fe/H] < -0.4$) clusters, age estimates remain absent. These clusters occupy a crucial regime for establishing the Galactic bulge age–metallicity relation. While the metal-rich end ($[Fe/H] > -0.4$) has been anchored by the detailed analysis of the twin metal-rich globular clusters NGC 6528 and NGC 6553 (S. Ortolani et al. 2025), and the moderately metal-poor end ($-1.4 < [Fe/H] < -1.0$) is constrained by the clusters studied in S. O. Souza et al. (2024, see their Table 3), the intermediate, moderately metal-rich regime has remained essentially unconstrained. With the present study of Tonantzintla 2, we are now finally able to close this long-standing gap.

Recently, S. Nepal et al. (2025) identified a chemically and kinematically distinct, pressure-supported spheroidal bulge component, characterized by a rapid early formation, a high-α sequence with minimal metallicity dependence, and a metallicity distribution function (MDF) sharply peaked at $[Fe/H] \approx -0.7$, most probably predating both the thick disk and the bar. The MDF peak they find thus defines the characteristic metallicity of the primordial bulge, offering a new framework for interpreting the origin of stellar systems in this metallicity regime.

In this work, we analyze color–magnitude diagrams (CMDs) of the globular cluster Tonantzintla 2 (hereafter Ton 2), having a metallicity of $[Fe/H] \sim -0.7$ (J. G. Fernández-Trincado et al. 2022), essentially identical to the MDF peak found in S. Nepal et al. (2025). While S. Nepal et al. (2025) used field stars and could not directly obtain ages for this spheroidal component, the authors speculate that the identified stellar population may represent the oldest fossil record of the Milky Way's assembly. By determining a precise age for Ton 2 in this same metallicity regime, we provide a direct constraint on the epoch at which the primordial bulge formed and refine the bulge age–metallicity relation in the critical interval it occupies.

Ton 2 was discovered by P. Pišmiš (1959) at the Tonantzintla Observatory in Mexico, using Schmidt photographic plates in the red. This allowed for the further detection of reddened bulge clusters. S. Djorgovski & G. Meylan (1993) presented revised coordinates. It is located at equatorial coordinates $(\alpha, \delta) = 17^{h}36^{m}10\overset{s}{.}5, -38°33'12\overset{''}{.}0$ and Galactic coordinates $(l, b) = 350\overset{°}{.}79645, -03\overset{°}{.}4233$. E. Bica et al.

(1996) analyzed V and I CMDs of Ton 2, deriving a distance to the Sun of $d_{\odot} = 6.4$ kpc, and a reddening of $E(B-V) = 1.26$. The unique thorough spectroscopic analysis of member stars carried out, from APOGEE spectra (S. R. Majewski et al. 2017), by J. G. Fernández-Trincado et al. (2022), resulted in a metallicity of [Fe/H] $= -0.70 \pm 0.05$. They also found a large spread of N abundances, which is also correlated with s-process (Ce) elements. Ton 2 shows a loose structure, with a concentration parameter of $c = 1.5$ (S. C. Trager et al. 1995).

Ton 2 has received different orbital classifications in the literature: it has been associated with the main bulge (V. Belokurov & A. Kravtsov 2024), with the thick disk (A. Pérez-Villegas et al. 2020), and as a low-energy cluster (D. Massari et al. 2019) or a possible member of the ancient Kraken accretion event (T. M. Callingham et al. 2022). These conflicting classifications clearly highlight the need for firm age and chemical constraints in order to clarify its origin and connection to the early bulge.

In the present work, we carry out a CMD study of the globular cluster Ton 2, together with a complementary chemical abundance analysis aimed at establishing its origin within the in situ bulge population. In particular, we complement the existing APOGEE abundance measurements for seven cluster members with new determinations of manganese and aluminum, key elements for distinguishing between accreted and in situ stellar populations (P. Das et al. 2020). In Section 2, the observations and data reductions are described. In Section 3, isochrone fitting is applied to CMDs and described. In Section 4, the results, including chemodynamical constraints, are discussed. Concluding remarks are given in Section 5.

2. Observations and Data Reduction

Our analysis combines Hubble Space Telescope (HST) WFC3 and Advanced Camera for Surveys (ACS) photometry with ground-based FORS2/Very Large Telescope (VLT) observations, enabling proper-motion cleaning from two-epoch data and yielding a high-fidelity CMD that isolates the cluster's evolutionary sequences.

The HST observations were carried out during GO-14074 (PI: Cohen) in WFC3/IR filters F110W and F160W, with a total exposure time of ∼1271 s in each filter, and in ACS/WFC filter F606W (1 s + 4 × 495 s). The mean epoch of observations is 2016.48. Ground-based data were obtained with the FORS2 spectrograph at the VLT of the European Southern Observatory (ESO) during the ESO program 0113.D-0065 (PI: Monaco). In this work, we only adopted images in the R_SPECIAL filter collected during the night of 2024 July 5 (epoch 2024.51).

For HST data, we adopted the two-step procedure described in D. Nardiello et al. (2018a) to obtain the final astrophotometric catalog: all the images are first analyzed to extract positions and fluxes with the `hst1pass` routine and ad hoc point-spread functions (PSFs; J. Anderson 2022) from each image; we derived astrometric and photometric transformations between images and we adopted images, transformations and PSFs to analyze with KS2 (J. Anderson et al. 2008) all the images simultaneously to obtain deeper photometry and precise positions and magnitudes. We cleaned the final catalog from bad measurements by using the diagnostics output of the data reduction, as done in D. Nardiello et al. (2018b).

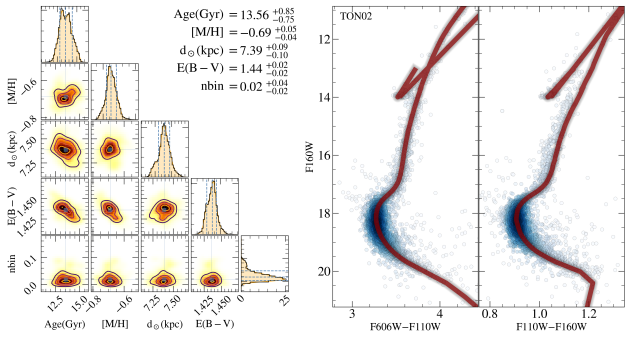

Figure 1. Ton 2 F160W versus F606W–F160W and F160W versus F110W–F160W CMDs (right panels), and corner plot of the parameters (left panels). A best fit was found for age of $13.56^{+0.85}_{-0.75}$ Gyr, [M/H] $= -0.69^{+0.05}_{-0.04}$, $d_{\odot} = 7.39^{+0.09}_{-0.19}$ kpc, and $E(B-V) = 1.44 \pm 0.02$.

FORS2 data were reduced by using the software described in D. Nardiello et al. (2015), that are based on the use of empirical PSFs and neighbor subtraction. We derived the geometric distortion of the two FORS2 CCDs by using the procedure described by M. Griggio et al. (2022).

For Ton 2, we calculated the displacements of the stars between the first and second epoch following the method presented in M. Libralato et al. (2021), which is based on the use of a network of cluster bona fide stars that allows local transformations. Using the same philosophy, we corrected the differential reddening that affects the magnitudes of Ton 2 stars as described in A. P. Milone et al. (2012).

3. Color–Magnitude Diagrams and Isochrone Fitting

The isochrone fitting procedure, carried out with the code SIRIUS (S. O. Souza et al. 2020), is also well-detailed in S. O. Souza et al. (2023, 2024) and S. Ortolani et al. (2025). The code enables us to derive the fundamental parameters such as age, metallicity, distance, reddening, and total-to-selective extinction ratio (R_V). The PAdova and TRieste Stellar Evolution Code[10] (PARSEC; A. Bressan et al. 2012) isochrones were used to build the synthetic diagrams. More details are given in Appendix A.

The two proper-motion-cleaned CMDs are shown in Figure 1, using the ACS wide-field camera, with filter F606W, and the WFC3 camera with filters F110W and F160W. The simultaneous fit of F160W versus F606W–F160W, and F160W versus F110W–F160W CMDs allows us to derive the proper value of the reddening law R_V (C. Pallanca et al. 2021).

The resulting combined fit yields an age of $13.58^{0.72}_{-1.0}$ Gyr, where internal uncertainties of the Bayesian method are assumed. A reddening of $E(B-V) = 1.44 \pm 0.02$, a metallicity of [M/H] $= -0.68$, a distance from the Sun of $d_{\odot} = 7.38^{0.13}_{0.08}$ kpc, and $R_V = 2.9 \pm 0.1$ are obtained.

The total-to-selective absorption parameter $R_V = 2.9$ is somewhat lower than the standard value of 3.1, which is compatible with the location of the cluster at about 3.°4 below the Galactic plane. As a matter of fact, the extinction maps by R. Zhang et al. (2023) indicate similar values ($2.9 < (R_V < 3.0)$) for the symmetric side of the bulge. We note that, from the same method of fitting CMDs in the optical and near-infrared, we derived $R_V = 2.6$ for Palomar 6 (S. O. Souza et al. 2021), and $R_V = 2.84 \pm 0.02$ for NGC 6355 (S. O. Souza et al. 2023).

[10] Version 3.8, https://stev.oapd.inaf.it/cgi-bin/cmd_3.8.

Table 1
Literature Ages of Oldest Bulge Clusters and Isochrone Sets Employed

Cluster	[Fe/H]	Age (Gyr)	References	Isochrone
NGC 6316	-0.92 ± 0.07	$13.4^{+0.6}_{-0.5}$	(1)	PARSEC
NGC 6355	-1.39 ± 0.08	13.2 ± 1.1	(2)	DSED
NGC 6401	-1.15 ± 0.20	13.2 ± 1.2	(3)	relative ages
NGC 6440	-0.5 ± 0.03	13.0 ± 1.5	(4)	DSED/PARSEC
NGC 6453	-1.48 ± 0.14	13.3 ± 0.8	(3)	relative ages
NGC 6717	-1.17 ± 0.09	$13.5^{+0.67}_{0.76}$	(5)	DSED/BaSTI
UKS 1	-0.98 ± 0.11	$13.1^{+0.93}_{-1.29}$	(6)	DSED
ESO 452-11	$-0.80^{+0.08}_{-0.11}$	$13.59^{+0.48}_{-0.69}$	(7)	BaSTI

References: 1. D. Deras et al. (2023); 2. S. O. Souza et al. (2023); 3. R. E. Cohen et al. (2021); 4. C. Pallanca et al. (2021); 5. R. A. P. Oliveira et al. (2020); 6. J. G. Fernández-Trincado et al. (2020); 7. D. Massari et al. (2025).

Finally, the age of 13.6 Gyr is the oldest of all analyzed bulge clusters so far, and it will be further discussed in the age–metallicity subsection below.

4. Discussion

In this section, we discuss the cluster orbits, chemical composition, and its old age. In Appendix B, we report literature ages, reddening $E(B-V)$, and distances and metallicities of Ton 2. For completeness, W. E. Harris (1996) reports a radial velocity of -184.4 km s^{-1}.

4.1. Orbits: A Bulge Cluster

The orbits were computed to derive the orbital parameters: the apogalactic distance $r_{\rm apo}$, perigalactic distance $r_{\rm peri}$, eccentricity ecc, maximum absolute height relative to the disk $|Z|_{\rm max}$, the energy $E_{\rm T}$, and the angular momentum $L_{\rm Z}$.

For the orbital integration, we adopted the analytical approximation given by M. C. Sormani et al. (2022) for the M. Portail et al. (2017) potential, with the Action-based GAlaxy Modelling Architecture (E. Vasiliev 2019). The results:

$r_{\rm apo}$: 4.25 ± 0.46
$r_{\rm peri}$: 1.03 ± 0.23
ecc: 0.63 ± 0.08
$|Z|_{\rm max}$: 2.19 ± 0.09
$E_{\rm T} \times 10^5$: -1.09 ± 0.02
$L_{\rm Z} \times 10^3$: -0.40 ± 0.05

showing that the cluster orbit is contained in the bulge volume. For reference, S. Nepal et al. (2025) found that the maximum extension of the spheroidal bulge is defined as $r_{\rm apo} < 5$ kpc, $|Z_{\rm max}| < 3$ kpc, and higher density for ecc > 0.7.

4.2. Age–Metallicity Plane: The Oldest Bulge Cluster?

In Table 1, we report bulge globular clusters with ages higher than 13.0 Gyr. As reported in E. Bica et al. (2024), only studies with resolved photometry, and most of them based on HST, or Gemini/GSAOI near-infrared photometry, are considered. The exception is UKS 1 based on the Vista Variables in the Via Lactea (VVV; D. Minniti et al. 2010) data. We also indicate the isochrone set employed, namely, Dartmouth or DSED (A. Dotter et al. 2008), PARSEC (A. Bressan et al. 2012), and BaSTI A. Pietrinferni et al. (2006, 2021). R. E. Cohen et al. (2021) used no isochrone sets but derived relative ages by comparing CMD fiducial lines of well-known clusters with those of their sample clusters. As for the ages reported in E. Bica et al. (2024), these same sets of isochrones were used, as well as the Victoria-Regina code and isochrones (D. A. VandenBerg et al. 2014), in a few cases.

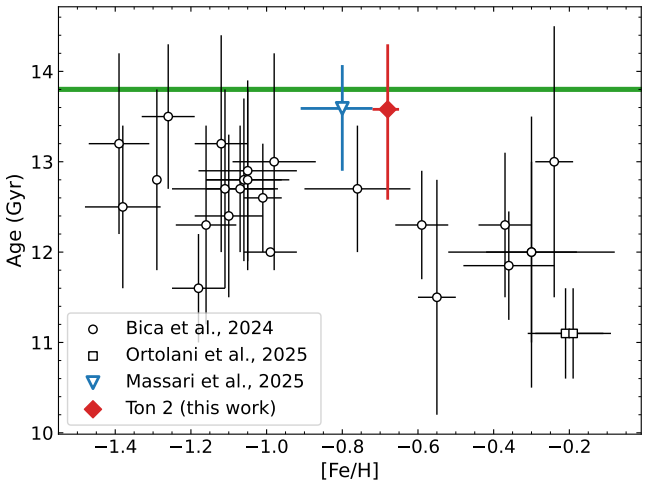

Figure 2. Age versus metallicity plane for bulge-volume clusters, highlighting the location of Ton 2. (The values are from E. Bica et al. 2024; D. Massari et al. 2025; S. Ortolani et al. 2025). The green line represents the age of the Universe of 13.801 ± 0.024 Gyr according to Planck Collaboration et al. (2020), with width showing the uncertainty.

Figure 2 shows the metallicities and ages of bulge globular clusters reported in E. Bica et al. (2024), the twin metal-rich clusters by S. Ortolani et al. (2025), and the location of Ton 2. We also show the cluster ESO 452-11 to which D. Massari et al. (2025) assign an age of $13.59^{+0.48}_{-0.69}$ Gyr.

The position of Ton 2 in the age–metallicity plane for bulge clusters is striking. Ton 2 appears to have formed very early during the Galaxy formation. It should be a representative of the protobulge. Ton 2 appears to be older than all clusters, with age only comparable to that of ESO 452-11, another bulge globular cluster with similar metallicity and therefore another potential bulge relic (although its in situ origin should still be demonstrated via a detailed chemical analysis, similar to that present here for Ton 2 in the next section). Although D. Massari et al. (2025) report an age of $13.59^{+0.48}_{-0.69}$ Gyr, the use of BaSTI isochrones (A. Pietrinferni et al. 2006, 2021) leads to systematically older ages as discussed in L. O. Kerber et al. (2018) and G. A. Gontcharov et al. (2019, 2020). In Appendix C, we show that from a comparison of BaSTI (A. Pietrinferni et al. 2006, 2021), DSED (A. Dotter et al. 2008), and PARSEC (A. Bressan et al. 2012), the results show an age difference of 0.4 dex higher for BaSTI relative to the other models. In addition, it would be important to know the chemical properties of ESO 452-11 to confirm its in situ origin.

4.3. Chemical Abundances: An In Situ Bulge Cluster

The unique spectroscopic analysis of member stars of Ton 2 was carried out by J. G. Fernández-Trincado et al. (2022). The spectra were obtained within the Apache Point Observatory Galactic Evolution Experiment II survey (APOGEE-2), obtained as part of the bulge Cluster APOgee Survey (D. Geisler et al. 2025). The seven stars analyzed resulted in a mean metallicity of [Fe/H] $= -0.70$, and alpha-element enhancements, with mean values [Mg/Fe] $= +0.29$, [Si/Fe] $= +0.33$, [Ca/Fe] $= +0.27$.

Table 2
Metallicities and Chemical Abundances for Ton 2, from J. G. Fernández-Trincado et al. (2022), C, N, and O from B. Barbuy et al. (2025), and Na, Al, P, and Mn Computed in This Work (Referred to as Tw)

Star	[Fe/H]	[C/Fe] B25b	[N/Fe] B25b	[O/Fe] B25b	[Na/Fe] tw	[Mg/Fe] FT22	[Al/Fe] tw/FT22	[P/Fe] tw	[Mn/Fe] tw	[Ni/Fe] FT22
Ton2-2114	−0.73	+0.10	+1.10	+0.85	+0.60	+0.23	+0.50/+0.39	+0.39	−0.08	+0.09
Ton2-3304	−0.74	+0.25	+0.95	+0.80	+0.70	+0.33	+0.42/+0.42	+0.20	−0.12	+0.10
Ton2-3312	−0.55	+0.25	+0.50	+0.90	+0.15	+0.38	+0.32/+0.29	⋯	−0.35	−0.07
Ton2-4199	−0.77	+0.20	+0.80	+0.70	+0.75	+0.22	+0.49/+0.42	⋯	+0.00	+0.15
Ton2-4336	−0.69	+0.00	+1.10	+0.70	+0.70	+0.31	+0.52/+0.46	⋯	−0.10	+0.09
Ton2-4371	−0.65	+0.20	+0.34	+0.85	+0.25	+0.22	+0.00/+0.36	+0.20	−0.25	+0.01
Ton2-5151	−0.75	+0.10	+0.65	+0.55	+0.50	+0.30	+0.04/⋯	+0.30	−0.25	+0.09

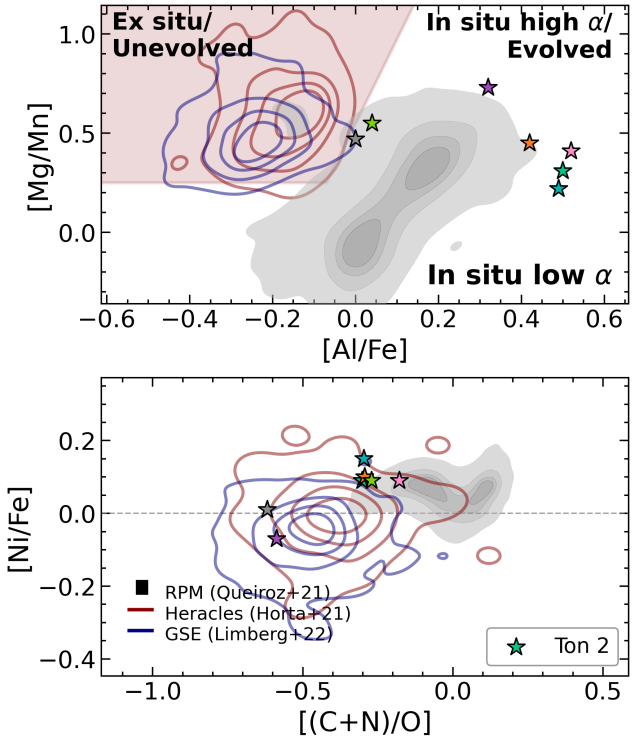

Figure 3. [Mg/Mn] versus [Al/Fe] (upper panel) and [Ni/Fe] versus [(C +N)/O]. Symbols: black-filled stars: star-members of Ton 2; brown lines: Heracles; and dark blue lines: GSE.

The alpha-like elements Al and Ti also show enhancements of [Al/Fe] = +0.39 and [Ti/Fe] = +0.29. N and O are also significantly enhanced. Finally, [Ce/Fe] shows some spread.

Table 2 reports the chemical abundances derived in J. G. Fernández-Trincado et al. (2022), together with C, N, O, and P analyzed in B. Barbuy et al. (2025), a remeasure of aluminum, as well as sodium and manganese (Mn) measured in the present work (see Appendix D).

Figure 3 (upper panel) shows [Mg/Mn] versus [Al/Fe] (P. Das et al. 2020) and [Ni/Fe] versus [(C+N)/O] (lower panel) (J. Montalbán et al. 2021; M. Ortigoza-Urdaneta et al. 2023) used to discriminate between in situ and ex situ origin. The location of the seven studied stars is compared with that of the reduced proper motion (RPM) sample of bona fide inner-galaxy stars from APOGEE (A. B. A. Queiroz et al. 2021), the accreted structures Gaia-Enceladus-Sausage (GSE; G. Limberg et al. 2022), and Heracles (D. Horta et al. 2021). In the upper panel, it is clear that the abundances of seven stars in Ton 2, given in Table 2, point toward an in situ origin of the cluster. In the lower panel, only one star shows [Ni/Fe] slightly negative, whereas all of the other six stars are enriched in Ni, again confirming the in situ origin of the cluster.

Another interesting further study of these APOGEE spectra was the detection of P-enrichment in part of the sample stars, for the clusters Tonantzintla 1 and NGC 6316, whereas for Ton 2, none in four stars has shown this effect (B. Barbuy et al. 2025), and for three stars, there is noise in the PI line region. In that work, we confirmed N and O enhancements, and also a correlation between [P/Fe] versus [N/O] in Tonantzintla 1 and NGC 6316. For Ton 2, we see a CNO-enhancement, likewise for these two other clusters. We note that a non–local thermodynamic equilibrium Al abundance would be about 0.1dex lower than the LTE value. A final comment is that some of the seven stars showing high N, O, and Na could be second-generation stars (see N. Bastian & C. Lardo 2018) of this cluster (e.g., J. G. Fernández-Trincado et al. 2020).

Another important indicator is the rather high Al abundance, which points toward an in situ origin of these clusters (S. Mészáros et al. 2020). This contradicts the suggestion by T. M. Callingham et al. (2022) that ranked Ton 2 as having origin in the Kraken structure, which otherwise was not included as a Kraken member in J. M. D. Kruijssen et al. (2020).

5. Conclusions

Our multiband HST photometry and high-resolution chemical analysis provide the most precise age derivation to date of the bulge globular cluster Tonantzintla 2. We derived a distance of $7.38^{+0.13}_{-0.08}$ kpc, and showed that its orbit is fully confined within the Galactic bulge. Isochrone fitting of proper-motion-cleaned CMDs yields an age of $13.58^{+0.72}_{-1.0}$ Gyr, placing Ton 2 among the oldest stellar systems known in the Milky Way, and the oldest so far in the Galactic bulge. At its metallicity of [Fe/H] = –0.7, Ton 2 sits exactly at the peak of the spheroidal and high-alpha stellar population, a primordial bulge component recently identified from field stars by S. Nepal et al. (2025), providing a direct age measurement for this population. A detailed high-resolution chemical abundance analysis of seven confirmed member stars, for which we determined manganese abundances—an element crucial in helping distinguish in situ from accreted stellar populations—complements our analysis. We find that the chemical abundance pattern—enhanced α-elements, high Al, N, and Ni, and elevated [Mg/Mn]—is fully consistent with an in situ origin and incompatible with an accreted structure origin such as Kraken.

These results show that the bulge reached the moderate metallicity of [Fe/H] $\simeq$–0.7 extremely early, within 200 million years from the Big Bang (Planck Collaboration et al. 2020). Ton 2 therefore represents a fossil remnant of the protobulge. Its properties (age and metallicity) remind those of

bulges and protoglobular clusters, as N-emitters now observed by JWST beyond redshift six (I. Morel et al. 2025). This suggests that the Milky Way experienced a similar rapid, early bulge-building phase, linking local relics such as Ton 2 with the processes driving galaxy assembly and chemical enrichment very early on in the history of the Universe.

Our work therefore provides, for the first time, the chemical and chronological framework that links this population of very old, moderately metal-poor bulge clusters to the metallicity peak ([Fe/H] $\simeq$ –0.7) of the primordial bulge. Ton 2 becomes the oldest globular cluster for which this connection can be demonstrated directly.

Acknowledgments

B.B. and E.B. acknowledge partial financial support from FAPESP, CNPq, and CAPES—Financial code 001. C.C. acknowledges partial financial support from FAPESP, project 2025/01915-0. S.O.S. acknowledges the DGAPA–PAPIIT grant IA103224 and the support from Dr. Nadine Neumayer's Lise Meitner grant from the Max Planck Society. J.G.F.-T. gratefully acknowledges the grant support provided by ANID Fondecyt Regular No. 1260371, ANID Fondecyt Postdoc No. 3230001 (Sponsoring researcher), the Joint Committee ESO-Government of Chile under the agreement 2023 ORP 062/2023, and the support of the Doctoral Program in Artificial Intelligence, DISC-UCN. This study was financed, in part, by the São Paulo Research Foundation (FAPESP), Brazil; Process No. 2025/05050-3. This research is based on observations made with the NASA/ESA Hubble Space Telescope obtained from the Space Telescope Science Institute, which is operated by the Association of Universities for Research in Astronomy, Inc., under NASA contract NAS 5–26555. The HST observations are associated with program GO-14074 (PI: Cohen). The data presented in this Letter were obtained from the Mikulski Archive for Space Telescopes (MAST) at the Space Telescope Science Institute. The specific observations analyzed can be accessed via MAST at doi:10.17909/t9-na33-8504. Ground-based data were obtained at the FORS2@VLT spectrograph, during the European Southern Observatory program 0113.D-0065 (PI: Monaco). Funding for the Sloan Digital Sky Survey IV has been provided by the Alfred P. Sloan Foundation, the U.S. Department of Energy Office of Science, and the Participating Institutions. SDSS-IV acknowledges support and resources from the Center for High-Performance Computing at the University of Utah. The SDSS website is https://www.sdss.org/.

Author Contributions

All authors contributed equally to this project.

Appendix A
The Code Sirius

The code SIRIUS (S. O. Souza et al. 2020), employed here to derive the age of Tonantzintla 2, adopts the Bayesian Markov Chain Monte Carlo (MCMC) method to obtain probability distributions for each parameter by comparing the observed CMDs with synthetic CMDs built from each set of parameters randomly, during the fitting process. The MCMC was applied using the `Python` library, `emcee` (D. Foreman-Mackey et al. 2013), and `PyDE`,[11] a global optimization that uses differential evolution. The PARSEC isochrones are adopted (A. Bressan et al. 2012). The parameter space spans ages between 7 and 14 Gyr with intervals of 0.1 Gyr, and metallicities between −2.0 and + 0.3 with intervals of 0.05 dex. For each MCMC realization, interpolations in the isochrone grid are carried out, assuming the initial mass function from P. Kroupa (2001). The synthetic CMDs use magnitudes from the PARSEC isochrone grid according to the parameters selected at each MCMC step. A fraction of unresolved binaries is adopted. The secondary components are assigned using a randomly selected mass ratio, and their combined magnitudes are computed by summing their fluxes. A magnitude-dependent error function derived from the observed photometric errors is applied at the position of the turn-off to preserve alignment with the observed CMD, simulating observational uncertainties. The extinction correction is computed at each iteration, applying the extinction law of J. A. Cardelli et al. (1989) for a determined R_V value. The observed distribution of stars in magnitude space results from the luminosity function applied to the synthetic sample.

[11] https://github.com/hpparvi/PyDE

Appendix B
Previous Literature on Tonantzintla 2

Literature values of reddening of $1.26 < E(B-V) < 1.23$ were adopted by W. E. Harris (1996), E. Bica et al. (1996), C. M. Dutra & E. Bica (2000), S. Vásquez et al. (2018), and D. Geisler et al. (2023), whereas $E(B-V) = 1.41^{+0.5}_{-0.1}$ was given by E. F. Schlafly & D. P. Finkbeiner (2011), the latter coinciding with our resulting value of $E(B-V) = 1.44 \pm 0.02$. We note that there is a strong reddening variation across the field. This explains why in Figure 1 we see two peaks in $E(B-V)$ and in age.

E. Vasiliev & H. Baumgardt (2021) estimate a distance to the Sun of $d_\odot = 5.9 \pm 0.6$ computed from Gaia data, whereas H. Baumgardt & E. Vasiliev (2021) give $d_\odot = 6.987 \pm 0.34$ based on a combination of several measurements, including Gaia data. We find a slightly larger distance of $d_\odot = 7.38^{+0.13}_{-0.08}$, a distance closer to the Galactic center, and clearly in the bulge volume.

S. Vásquez et al. (2018) and D. Geisler et al. (2023) derived metallicities of -0.73 ± 0.13 and -0.61 ± 0.03, respectively, from the Ca II triplet lines, whereas a thorough spectroscopic analysis by J. G. Fernández-Trincado et al. (2022, F-T22) resulted in a metallicity of [Fe/H] $= -0.70 \pm 0.05$. Our derived value of [M/H] $= -0.68^{+0.04}_{-0.08}$ is somewhat lower than that of F-T22, given that it takes into account the alpha-enhancement around [α/Fe] $= +0.4$ (F-T22).

Appendix C
Age versus Different Isochrone Sets

To illustrate the difference in age as derived from different isochrone sets, in Figure 4, we carried out a comparison of BaSTI isochrones (A. Pietrinferni et al. 2006) of ages 13.5 and 12.5 Gyr and [Fe/H] $= -0.7$ fitted by DSED isochrones (A. Dotter et al. 2008), giving $13.11^{+0.30}_{-0.28}$ and $12.17^{+0.29}_{-0.31}$, respectively. For Ton 2's metallicity ([Fe/H] $= -0.70$), there is a very good match between BaSTI and DSED in the main-sequence turn-off and subgiant branch (MSTO+SGB), but for a 0.4 Gyr younger DSED isochrone, representing a systematic difference.

For a comparison with PARSEC A. Bressan et al. (2012) isochrones, resulting in: 1) The red giant branch tilting is the

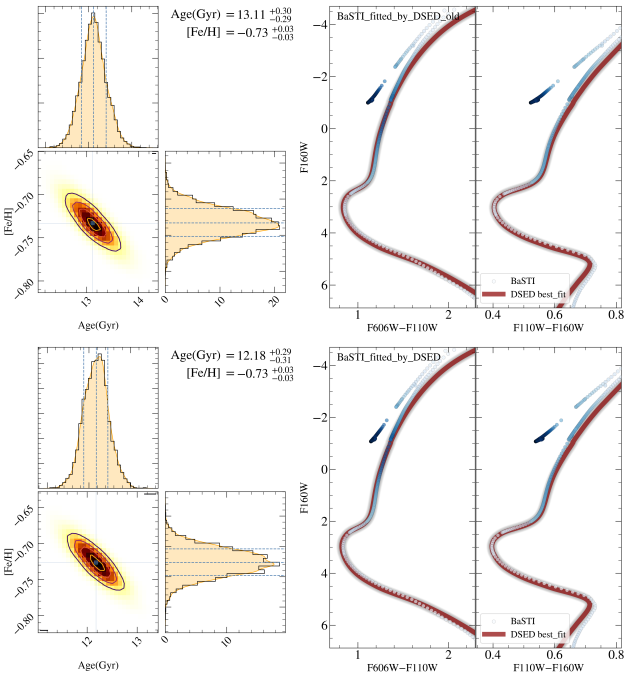

Figure 4. BaSTI isochrones of 13.5 and 12.5 Gyr, fitted with DSED isochrones, and corresponding age.

largest difference. BaSTI is steeper, eventually in better agreement with our data, but this is not the case near the SGB base. A younger BaSTI gives the best fit to PARSEC. 2) Turn-off (TO) shows a shift. It is not obvious if BaSTI gives an older or younger age. Shifting and forcing the fit to PARSEC eventually will lead to a best fit with 13.5 Gyr. 3) The largest discrepancy is the horizontal branch (HB). BaSTI is too faint, and an older age is needed to simultaneously fit HB and TO. Consequently, since D. Massari et al. (2025) used the HB fit, they found an older age relative to PARSEC. Finally, the data for ESO 452–11 are not clean from field stars; therefore, the age derivation is uncertain.

Appendix D
Manganese Abundances

In order to analyze indicators of stellar populations ex situ or in situ, we derived Mn abundances. We also rederived Al and Na abundances. The code Turbospectrum for spectrum synthesis is used (B. Plez 2012).

Figure 5 shows the fit to the three Mn lines MnI 15159.200, 15217.793, and 15262.702 Å in star Ton 2: 2M17361421-3834371, illustrating the good quality of the fit, and therefore of the Mn abundances. We also rederived the abundances of Na and Al from the lines NaI 16388.85 Å, and AlI 16718.957, 16750.539, and 16763.359 Å lines.

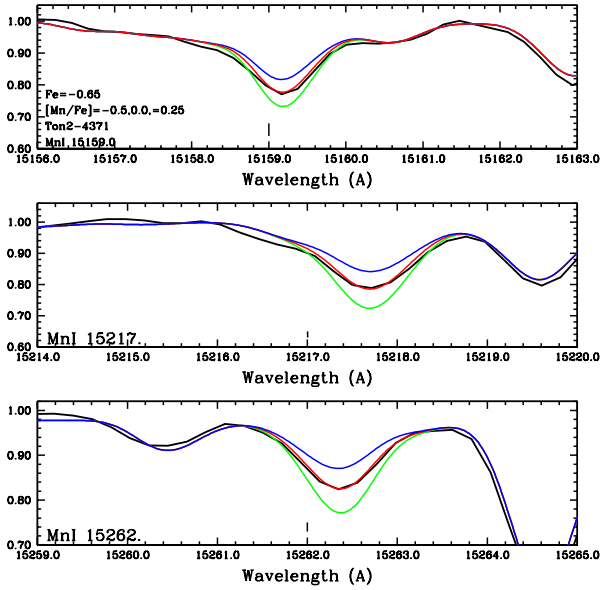

Figure 5. Fit to Mn lines for star Ton 2: 2M17361421-383431.

ORCID iDs

Sergio Ortolani https://orcid.org/0000-0001-7939-5348
Stefano O. Souza https://orcid.org/0000-0001-8052-969X
Domenico Nardiello https://orcid.org/0000-0003-1149-3659
Beatriz Barbuy https://orcid.org/0000-0001-9264-4417
Eduardo Bica https://orcid.org/0000-0003-3336-0910
Bernardo P.L. Ferreira https://orcid.org/0000-0002-7552-3063
Cristina Chiappini https://orcid.org/0000-0003-1269-7282
José G. Fernández-Trincado https://orcid.org/0000-0003-3526-5052
Heitor Ernandes https://orcid.org/0000-0001-6541-1933

References

Anderson, J. 2022, One-Pass HST Photometry with hst1pass, Instrument Science Report WFC3 2022-5, 55
Anderson, J., King, I. R., Richer, H. B., et al. 2008, AJ, 135, 2114
Barbuy, B., Fernández-Trincado, J. G., Camargo, M. S., et al. 2025, AJ, 170, 245
Bastian, N., & Lardo, C. 2018, ARA&A, 56, 83
Baumgardt, H., & Vasiliev, E. 2021, MNRAS, 505, 5957
Belokurov, V., & Kravtsov, A. 2024, MNRAS, 528, 3198
Bica, E., Ortolani, S., & Barbuy, B. 1996, A&AS, 120, 153
Bica, E., Ortolani, S., Barbuy, B., & Oliveira, R. A. P. 2024, A&A, 687, A201
Bressan, A., Marigo, P., Girardi, L., et al. 2012, MNRAS, 427, 127
Callingham, T. M., Cautun, M., Deason, A. J., et al. 2022, MNRAS, 513, 4107
Cardelli, J. A., Clayton, G. C., & Mathis, J. S. 1989, ApJ, 345, 245
Cohen, R. E., Bellini, A., Casagrande, L., et al. 2021, AJ, 162, 228
Das, P., Hawkins, K., & Jofré, P. 2020, MNRAS, 493, 5195
Deras, D., Cadelano, M., Ferraro, F. R., Lanzoni, B., & Pallanca, C. 2023, ApJ, 942, 104
Djorgovski, S., & Meylan, G. 1993, ASPC, 50, 325
Dotter, A., Chaboyer, B., Jevremović, D., et al. 2008, ApJS, 178, 89
Dutra, C. M., & Bica, E. 2000, A&A, 359, 347
Fernández-Trincado, J. G., Minniti, D., Beers, T. C., et al. 2020, A&A, 643, A145
Fernández-Trincado, J. G., Villanova, S., Geisler, D., et al. 2022, A&A, 658, A116
Foreman-Mackey, D., Hogg, D. W., Lang, D., & Goodman, J. 2013, PASP, 125, 306
Geisler, D., Muñoz, C., Villanova, S., et al. 2025, A&A, 703, A267
Geisler, D., Parisi, M. C., Dias, B., et al. 2023, A&A, 669, A115
Gontcharov, G. A., Khovritchev, M. Y., & Mosenkov, A. V. 2020, MNRAS, 497, 3674
Gontcharov, G. A., Mosenkov, A. V., & Khovritchev, M. Y. 2019, MNRAS, 483, 4949
Griggio, M., Bedin, L. R., Raddi, R., et al. 2022, MNRAS, 515, 1841
Harris, W. E. 1996, AJ, 112, 1487
Horta, D., Schiavon, R. P., Mackereth, J. T., et al. 2021, MNRAS, 500, 1385
Kerber, L. O., Nardiello, D., Ortolani, S., et al. 2018, ApJ, 853, 15
Kroupa, P. 2001, MNRAS, 322, 231
Kruijssen, J. M. D., Pfeffer, J. L., Chevance, M., et al. 2020, MNRAS, 498, 2472
Libralato, M., Lennon, D. J., Bellini, A., et al. 2021, MNRAS, 500, 3213
Limberg, G., Souza, S. O., Pérez-Villegas, A., et al. 2022, ApJ, 935, 109
Majewski, S. R., Schiavon, R. P., Frinchaboy, P. M., et al. 2017, AJ, 154, 94
Massari, D., Bellazzini, M., Libralato, M., et al. 2025, A&A, 698, A197
Massari, D., Koppelman, H. H., & Helmi, A. 2019, A&A, 630, L4
Mészáros, S., Masseron, T., García-Hernández, D. A., et al. 2020, MNRAS, 492, 1641
Milone, A. P., Marino, A. F., Cassisi, S., et al. 2012, ApJl, 754, L34
Minniti, D., Lucas, P. W., Emerson, J. P., et al. 2010, NewA, 15, 433
Montalbán, J., Mackereth, J. T., Miglio, A., et al. 2021, NatAs, 5, 640
Morel, I., Schaerer, D., Marques-Chaves, R., et al. 2025, arXiv:2511.20484
Nardiello, D., Libralato, M., Piotto, G., et al. 2018a, MNRAS, 481, 3382
Nardiello, D., Milone, A. P., Piotto, G., et al. 2015, A&A, 573, A70
Nardiello, D., Milone, A. P., Piotto, G., et al. 2018b, MNRAS, 477, 2004
Nepal, S., Chiappini, C., Pérez-Villegas, A., et al. 2025, arXiv:2507.06863
Oliveira, R. A. P., Souza, S. O., Kerber, L. O., et al. 2020, ApJ, 891, 37
Ortigoza-Urdaneta, M., Vieira, K., Fernández-Trincado, J. G., et al. 2023, A&A, 676, A140
Ortolani, S., Souza, S. O., Nardiello, D., Barbuy, B., & Bica, E. 2025, A&A, 698, A181
Pallanca, C., Lanzoni, B., Ferraro, F. R., et al. 2021, ApJ, 913, 137
Pérez-Villegas, A., Barbuy, B., Kerber, L. O., et al. 2020, MNRAS, 491, 3251
Pietrinferni, A., Cassisi, S., Salaris, M., & Castelli, F. 2006, ApJ, 642, 797
Pietrinferni, A., Hidalgo, S., Cassisi, S., et al. 2021, ApJ, 908, 102
Pišmiš, P. 1959, BOTT, 2, 37
Planck Collaboration, Aghanim, N., Akrami, Y., et al. 2020, A&A, 641, A6
Plez, B., 2012 Turbospectrum: Code for spectral synthesis, Astrophysics Source Code Library, ascl:1205.004
Portail, M., Gerhard, O., Wegg, C., & Ness, M. 2017, MNRAS, 465, 1621
Queiroz, A. B. A., Chiappini, C., Perez-Villegas, A., et al. 2021, A&A, 656, A156
Schlafly, E. F., & Finkbeiner, D. P. 2011, ApJ, 737, 103
Sormani, M. C., Gerhard, O., Portail, M., et al. 2022, MNRAS, 514, L1
Souza, S. O., Kerber, L. O., Barbuy, B., et al. 2020, ApJ, 890, 38
Souza, S. O., Ernandes, H., Valentini, M., et al. 2023, A&A, 671, A45
Souza, S. O., Libralato, M., Nardiello, D., et al. 2024, A&A, 690, A37
Souza, S. O., Valentini, M., Barbuy, B., et al. 2021, A&A, 656, A78
Trager, S. C., King, I. R., & Djorgovski, S. 1995, AJ, 109, 218
VandenBerg, D. A., Bergbusch, P. A., Ferguson, J. W., & Edvardsson, B. 2014, ApJ, 794, 72
Vasiliev, E. 2019, MNRAS, 482, 1525
Vasiliev, E., & Baumgardt, H. 2021, MNRAS, 505, 5978
Vásquez, S., Saviane, I., Held, E. V., et al. 2018, A&A, 619, A13
Zhang, R., Yuan, H., & Chen, B. 2023, ApJS, 269, 6